

Spectral oximetry assessed with high-speed ultra-high-resolution optical coherence tomography

Larry Kagemann

University of Pittsburgh School of Medicine
Department of Ophthalmology
Ophthalmology and Visual Sciences Research Center
UPMC Eye Center
Eye and Ear Institute
Pittsburgh, Pennsylvania 15213
and
University of Pittsburgh School of Engineering
Department of Bioengineering
Pittsburgh, Pennsylvania 15213

Gadi Wollstein

University of Pittsburgh School of Medicine
Department of Ophthalmology
Ophthalmology and Visual Sciences Research Center
UPMC Eye Center
Eye and Ear Institute
Pittsburgh, Pennsylvania 15213

Maciej Wojtkowski

Massachusetts Institute of Technology
Department of Electrical Engineering and Computer
Science
Research Laboratory of Electronics
Cambridge, Massachusetts 02139
and
Nicolaus Copernicus University
Institute of Physics
Torun, Poland 87-100

Hiroshi Ishikawa

University of Pittsburgh School of Medicine
Department of Ophthalmology
Ophthalmology and Visual Sciences Research Center
UPMC Eye Center
Eye and Ear Institute
Pittsburgh, Pennsylvania 15213
and
University of Pittsburgh School of Engineering
Department of Bioengineering
Pittsburgh, Pennsylvania 15213

Kelly A. Townsend

University of Pittsburgh School of Medicine
Department of Ophthalmology
Ophthalmology and Visual Sciences Research Center
UPMC Eye Center
Eye and Ear Institute
Pittsburgh, Pennsylvania 15213

Michelle L. Gabriele

University of Pittsburgh School of Medicine
Department of Ophthalmology
Ophthalmology and Visual Sciences Research Center
UPMC Eye Center
Eye and Ear Institute
Pittsburgh, Pennsylvania 15213
and
University of Pittsburgh School of Engineering
Department of Bioengineering
Pittsburgh, Pennsylvania 15213

Vivek J. Srinivasan

James G. Fujimoto
Massachusetts Institute of Technology
Department of Electrical Engineering and Computer
Science
Research Laboratory of Electronics
Cambridge, Massachusetts 02139

Joel S. Schuman

University of Pittsburgh School of Medicine
Department of Ophthalmology
Ophthalmology and Visual Sciences Research Center
UPMC Eye Center
Eye and Ear Institute
Pittsburgh, Pennsylvania 15213
and
University of Pittsburgh School of Engineering
Department of Bioengineering
Pittsburgh, Pennsylvania 15213

Abstract. We use Fourier domain optical coherence tomography (OCT) data to assess retinal blood oxygen saturation. Three-dimensional disk-centered retinal tissue volumes were assessed in 17 normal healthy subjects. After removing DC and low-frequency a-scan components, an OCT fundus image was created by integrating total reflectance into a single reflectance value. Thirty fringe patterns were sampled; 10 each from the edge of an artery, adjacent tissue, and the edge of a vein, respectively. A-scans were recalculated, zeroing the DC term in the power spectrum, and used for analysis. Optical density ratios (ODRs) were calculated as $ODR_{Art} = \ln(Tissue_{855}/Art_{855})/\ln(Tissue_{805}/Art_{805})$ and $ODR_{Vein} = \ln(Tissue_{855}/Vein_{855})/\ln(Tissue_{805}/Vein_{805})$ with Tissue, Art, and Vein representing total a-scan reflectance at the 805- or 855-nm centered bandwidth. Arterial and venous ODRs were compared by the Wilcoxon signed rank test. Arterial ODRs were significantly greater than venous ODRs (1.007 ± 2.611 and -1.434 ± 4.310 , respectively; $p=0.0217$) (mean \pm standard deviation). A difference between arterial and venous blood saturation was detected. This suggests that retinal oximetry may possibly be added as a metabolic measurement in structural imaging devices. © 2007 Society of Photo-Optical Instrumentation Engineers. [DOI: 10.1117/1.2772655]

Keywords: spectroscopy; retina; metabolism; oximetry; oxygen; optical coherence tomography.

Paper 06316SSRRR received Nov. 7, 2006; revised manuscript received Jun. 11, 2007 and Jul. 16, 2007; accepted for publication Jul. 16, 2007; published online Aug. 13, 2007.

1 Introduction

Quantification of the oxygen saturation of hemoglobin within the vasculature of the eye would be useful in the study and management of a number of diseases associated with regional

Address all correspondence to Joel S. Schuman, University of Pittsburgh School of Medicine, UPMC Eye Center, Eye and Ear Institute, 203 Lothrop St., Suite 816, Pittsburgh, PA 15213. Tel: (412) 647-2205; Fax: (412) 647-5119; E-mail: Schumanjs@upmc.edu

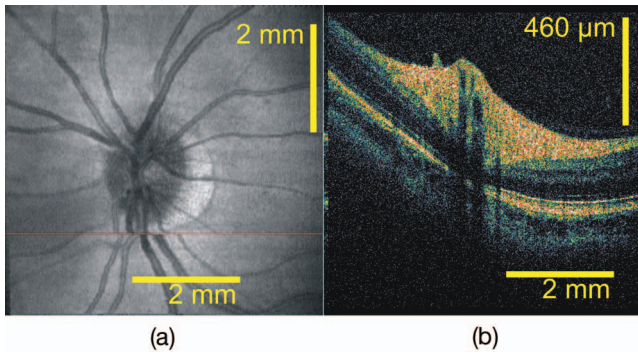


Fig. 1 OCT fundus image of a 3-D optic-nerve-head-centered raster scan. The red line on the OCT fundus image (a) shows the location of the cross-section slice in (b). A motion artifact occurred during imaging, creating the discontinuity in the blood vessels observed at the red line in (a).

ischemia and infarct such as diabetic retinopathy,¹ ocular vasculopathies such as anterior ischemic optic neuropathy,² and central and retinal branch artery and vein occlusion.³ For this reason, there have been numerous attempts to develop a spectral technique for the assessment of retinal blood oxygenation dating back to the early 1960s.⁴⁻¹⁰ Preliminary data suggests that spectral techniques may be applicable in recently developed spectroscopic optical coherence tomography technology.¹¹⁻¹³

All spectral reflectance methods are based on assumptions about the relationship between light transmittance and oxygen saturation,¹⁴ which is expressed as

$$I = I_0 e^{-(\epsilon * C * d)}, \quad (1)$$

where the intensity of light transmitted (I) through blood is equal to the original intensity (I_0) multiplied by e raised to the factor of a constant (ϵ) times distance traveled through blood (d) times concentration of blood (C). Solving for ϵ yields

$$\epsilon = 1/(C * d) * \ln(I_0/I), \quad (2)$$

where ϵ is the extinction coefficient, which is a term quantifying the combined effects of scattering and absorption per unit distance per unit concentration in a solution. Optical density (OD) is defined as the natural logarithm of (I_0/I).

Ultra-high-resolution¹⁵⁻²² and Fourier domain²³⁻²⁷ optical coherence tomography (OCT) are relatively new technologies that use a broad-spectrum light source. The devices acquire high-resolution images at high speed, which provides highly detailed information from the scanned area. Unlike other application-specific devices such as pulse oximeters, the retinal vessel analyzer that measures blood vessel diameter, or the Canon laser blood flowmeter that measures blood flow in specific retinal vessels, OCT scans of the retina have the potential to simultaneously assess tissue volume, blood flow within that tissue bed, and the oxygen saturation of the blood flowing within those vessels. Combined, OCT scans of the human retina have the potential to provide the only complete and precise assessment of metabolism in medicine. Our high-speed ultra-high-resolution Fourier domain OCT (hsUHR-

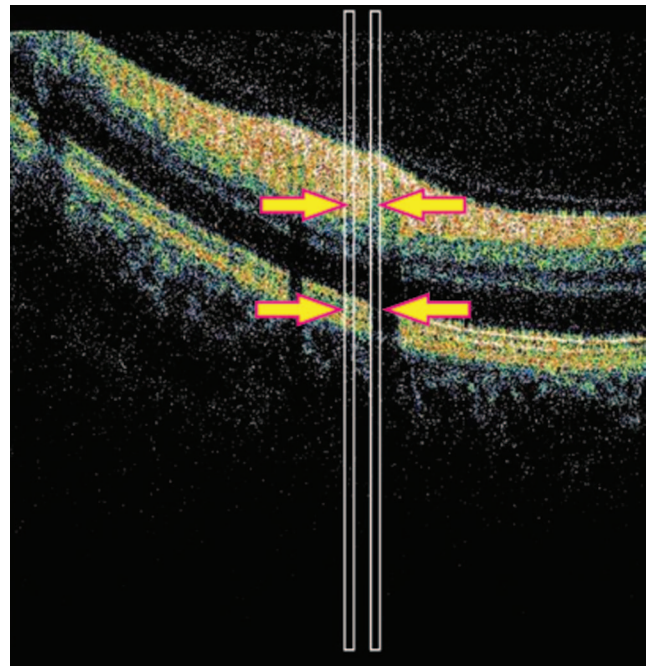


Fig. 4 The difference between adjacent a-scans located on (right) and off (left) of a blood vessel is loss of light due to interactions between light and blood, which is specifically the physical phenomenon that we desire to measure.

OCT) uses a light source that includes an oxyhemoglobin-deoxyhemoglobin isosbestic wavelength. Given the previous success of fundus camera-based systems, in which reflectance was quantified with no tissue depth resolution, an analysis of full axial content a-scans may provide sufficient data to quantify an oxygen sensitive optical density ratio (ODR).^{6,10} The purpose of the present study is to determine if the spectral data within hsUHR-OCT scans are suitable for the measurement of blood oxygen saturation measurements within retinal arteries and veins.

2 Methods

All procedures were approved by the institutional review board at the University of Pittsburgh School of Medicine. Informed consent was provided by all subjects before participa-

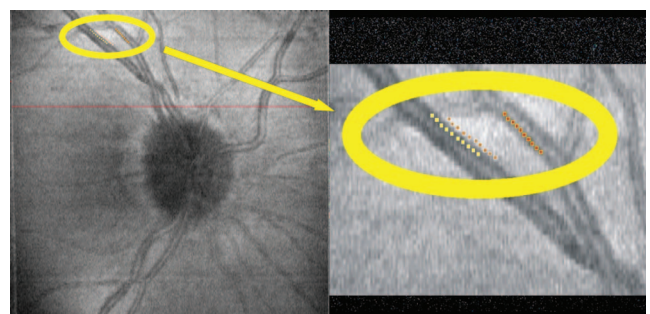


Fig. 6 Individual pixel optical densities were sampled from a vein (yellow), artery (red), and intervening tissue (orange), avoiding motion artifact and specular reflection.

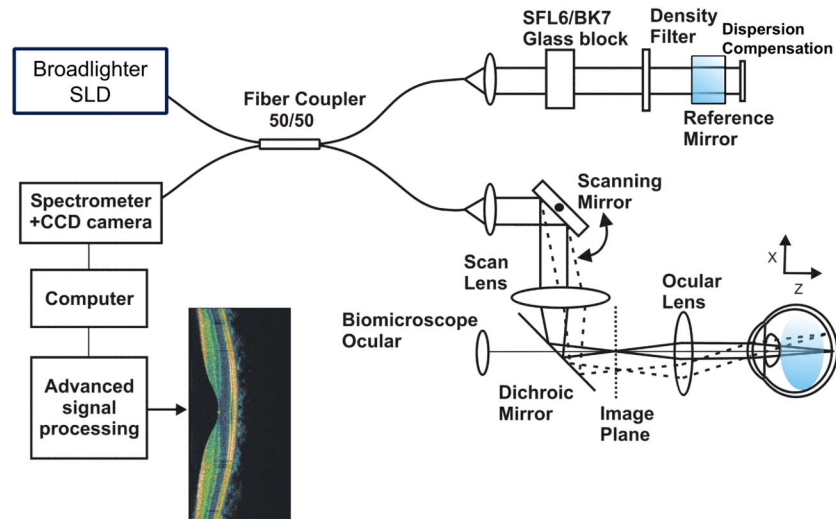


Fig. 2 Schematic drawing of the high-speed ultra-high-resolution optical coherence tomography system.

tion in the studies, and the study was conducted in compliance with the health insurance portability and accountability act.

2.1 Subjects

Seventeen subjects were recruited for the study. All subjects were recruited from the staff and faculty of the Eye and Ear Institute of the University of Pittsburgh Medical Center, and were normal healthy individuals with no history of ocular disease or trauma.

2.2 Instrumentation

The hsUHR-OCT may be used to image the layers of the retina (Fig. 1). Principles of the hsUHR-OCT have been described previously.^{23,24,28,29} Briefly, light from a 100-nm bandwidth low-coherence broadband light source (840 ± 50 nm, Broadlighter 840, SuperLum Diodes Ltd., Moscow, Russia) is split into two paths in a 50:50 fiber coupler. One beam is

projected onto a stationary reference mirror and the second was focused on and scanned the retina (Fig. 2). Light reflected from the mirror and the light backscattered from the retina are combined to form an interference pattern. Depth information describing the location of scattering structures within the retina is frequency-encoded in the spectral fringes.

Three dimensional (3-D) optic-disk-centered raster scans were obtained with the hsUHR-OCT device. Scans encompassed a 6×6 -mm slice of retinal tissue, with a total axial dimension of 1.34 mm. The 6×6 -mm area was scanned with a 180×512 -point array of a-scans (Fig. 1). Each a-scan contained 1024 axial pixels, and the axial resolution enabled by the source bandwidth was $\sim 3.4 \mu\text{m}$. Image quality was assessed subjectively and only good quality scans were used for the analysis. Specifically, OCT fundus images were assessed for the appearance of sharp vessel borders, suggesting good focus, and evenly spread vignetting, suggesting that the scan was positioned on the center of the field of view with minimal distortion due to eye movements or black lines due to blinking.

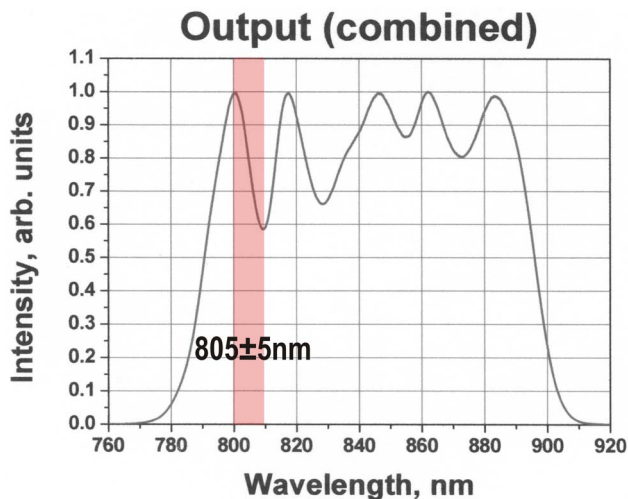


Fig. 3 The spectrum of the light source in our hsUHR-OCT contains distinct peaks at well-defined wavelengths. The band at 805 ± 5 nm has been highlighted.

3 Spectral Oximetry and Data Analysis

Data describing reflectance at specific wavelengths were obtained from structural optic-nerve-head (ONH)-centered hsUHR-OCT image data. The wavelengths measured by the CCD camera (Fig. 2) were calibrated by locating peaks within the light source spectrum provided by the manufacturer (Fig. 3). Customized code written in Labview (version 7.1, National Instruments, Inc., Austin, Texas) was used to identify the pixel location and bandwidth of the wavelengths of the light source. The light from our 100-nm bandwidth source was focused onto the central 1000 pixels of a 2048-pixel linear CCD camera, providing a spectral resolution with a theoretical limit of approximately 0.1 nm. Unlike the numerous spectral OCT systems utilizing a light source with a 50-nm bandwidth, the device in this study uses a light source with a bandwidth of 100 nm. This necessitates the sharpest possible focus of the spectral signal onto the linear CCD, and minimal spectral aberration. The utilization of a subset of all

available pixels on the CCD camera is due to the limitation in the optics available at the time of device construction. Sharp focus could not be obtained at any greater focal length, so the physically limited width is used. In order to sample light with a 10-nm range of a wavelength of interest, the 95 pixels surrounding that wavelength were analyzed. Zero-padding provided a-scans of 64 pixels for each narrow band of wavelengths sampled. For example, to measure light at 805 ± 5 nm, the pixels from 620 to 715 were sampled.

Determination of hemoglobin oxygen saturation requires quantification of the amount of light absorbed or scattered by blood within the retinal vasculature.¹¹ This was accomplished by comparing a-scans at the edges of blood vessels to adjacent a-scans off of the vessel (Fig. 4). Artery and vein pairs were located within the 2-D projection of the OCT fundus image. The unprocessed fringe data corresponding to pixels chosen for analysis within the OCT fundus image was identified. A-scans were recalculated, zeroing the constant term in the power spectrum, and used for analysis. Sampling vessels and tissue in close proximity ensured similar tissue thickness and pigment content between the two, leaving differences in reflections primarily due to interaction with blood, or the lack thereof. A-scans at the edge of the blood vessels, as opposed to the center of the blood vessels, were chosen to reduce the influence of specular reflection, and the use of the OCT fundus images allows identification of specific a-scans of interest. Light from the entire a-scan was summed in the spectral analysis with the assumption that the difference between total reflectance within these two a-scans was due primarily to light being scattered or absorbed by blood.³⁰ This approach mimics previous fundus camera techniques, and helps to remove the effects of local variations in absorption by other photoactive materials and the contributions of local tissue geometry to variations in reflectance.

Thirty sets of fringe data were sampled from each image. Ten fringe patterns were sampled from the edge of an artery, adjacent tissue, and the edge of a vein, respectively. Average light intensities for each of the 10 measurements for each subject were calculated, as were average intensities across all subjects for artery, vein, and tissue. Optical densities (ODs) and optical density ratios (ODRs) were calculated for each. Arteries and veins were identified by visual inspection of the OCT fundus image. It was required that sampled pixels be in an area of vessel or tissue with adequate illumination. As previously mentioned, in the case of vessel samples, pixels were required to be near the edge of the vessel in order to avoid specular reflection. Vessels were sampled in the plane of the fundus, outside of the ONH. OD is a measure of light absorbance relative to tissue surrounding a blood vessel,³¹ and is calculated as

$$OD_{\lambda} = \ln\left(\frac{I_{\lambda 0}}{I_{\lambda}}\right), \quad (3)$$

where I_{λ} and $I_{\lambda 0}$ are the average pixel values inside and immediately adjacent to a blood vessel when illuminated at wavelength λ . The extinction coefficients of oxyhemoglobin and deoxyhemoglobin vary with wavelength (Fig. 5).³² For example, light at 805 nm is equally scattered by oxyhemoglobin and deoxyhemoglobin, and for this reason is defined as an isosbestic wavelength. Ratios of ODs (ODR) between those

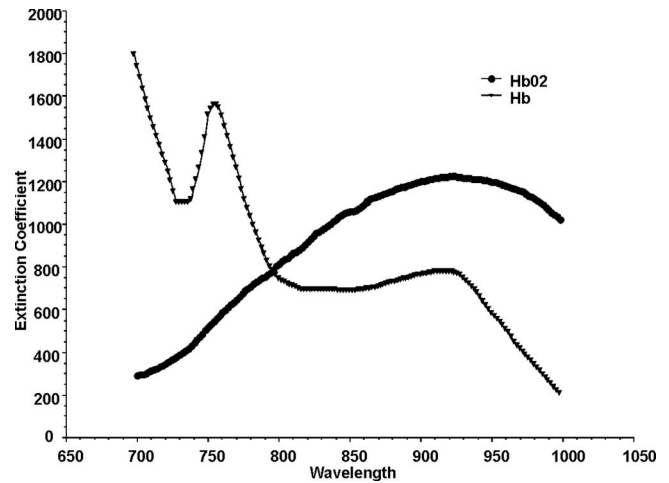


Fig. 5 Oxy- and deoxyhemoglobin absorb and scatter light with different magnitudes across much of the spectrum of our light source.

measured at oxygen sensitive wavelengths and isosbestic wavelengths are linearly proportional to blood oxygen saturation.³⁰ This is expressed as:

$$SO_2 = (a + b) \left(\frac{OD_{\text{sensitive}}}{OD_{\text{isosbestic}}} \right) = (a + b) ODR, \quad (4)$$

where SO_2 is percent hemoglobin oxygen saturation, a and b are constants, $OD_{\text{sensitive}}$ and $OD_{\text{isosbestic}}$ are optical densities at oxygen sensitive and insensitive wavelengths, respectively, and ODR is the optical density ratio. In the present study, 805 ± 5 nm was used as the isosbestic wavelength, and 855 ± 5 nm was used as the oxygen sensitive wavelength. Here, 855 nm was selected because it is a location in the spectrum where the difference in extinction coefficients between oxyhemoglobin and deoxyhemoglobin is relatively large within the available bandwidth.

Mean light intensities for each parameter for each subject were calculated. The coefficients of variation for light intensities for each parameter for each subject were calculated. Ninety-five pixels presenting 12-bit data were summed to measure light intensity in the bandwidths of interest, representing a potential intensity signal of 389,120. In order to obtain an estimate of signal strength, the average intensity measurements for all parameters as a percentage of CCD light saturation level was also calculated. Arterial and venous ODRs, calculated from the average intensities across all subjects, were compared by the Wilcoxon signed rank test. P values less than or equal to 0.05 were considered significant.

4 Results

Seventeen normal healthy subjects (nine female, eight male, ages 40 ± 7 years) were recruited for the study. Ophthalmic normalcy had been established by subject participation in prior studies. All subjects were successfully examined by hsUHR-OCT using the 3-D protocol. Images were of sufficient quality to allow sampling of 10 pixels on an artery, 10 pixels on a vein, and 10 pixels on tissue between an artery and vein, while avoiding motion artifacts (Fig. 6). Eleven of 17 eyes presented with higher oxygen saturation observed in

Table 1 The “mean” values are the averages of the light intensity within the respective bandwidths (isosbestic and oxygen sensitive). OD values are calculated as the natural log of the ratio of tissue to vessel light intensity for the perspective bandwidths. Positive ODR Art–ODR Vein differences represent subjects in which arterial blood oxygen saturation was higher than venous oxygen saturation. Coefficients of variation for each of the parameters, calculated from the mean and standard deviation of the 10 measurements, are presented.

	Subject									
	1	2	3	4	5	6	7	8	9	10
Mean Artery Isosbestic	19.14	48.88	61.74	45.87	52.58	72.41	34.18	56.02	27.71	39.24
Mean Artery Sensitive	19.23	60.42	82.47	69.90	45.56	75.14	35.45	63.68	39.80	41.97
Mean Vein Isosbestic	15.81	48.69	51.32	50.77	54.18	66.92	32.64	63.39	24.38	35.78
Mean Vein Sensitive	14.46	68.68	68.92	71.16	43.68	72.66	37.56	71.51	36.02	44.32
Mean Tissue Isosbestic	15.26	44.30	55.51	47.27	50.89	65.33	34.44	59.04	23.98	32.84
Mean Tissue Sensitive	18.67	61.00	67.93	73.05	41.79	73.77	37.70	71.93	38.24	44.40
OD Artery Isosbestic	-0.23	-0.10	-0.11	0.03	-0.03	-0.10	0.01	0.05	-0.14	-0.18
OD Artery Sensitive	-0.03	0.01	-0.19	0.04	-0.09	-0.02	0.06	0.12	-0.04	0.06
ODR Artery	0.13	-0.10	1.82	1.47	2.65	0.18	8.38	2.32	0.28	-0.32
OD Vein Isosbestic	-0.04	-0.09	0.08	-0.07	-0.06	-0.02	0.05	-0.07	-0.02	-0.09
OD Vein Sensitive	0.26	-0.12	-0.01	0.03	-0.04	0.02	0.00	0.01	0.06	0.00
ODR Vein	-7.17	1.26	-0.19	-0.37	0.71	-0.63	0.07	-0.08	-3.57	-0.02
ODR Art–ODR Vein	7.30	-1.35	2.01	1.83	1.94	0.81	8.31	2.40	3.85	-0.30
Coefficient of Variation Artery Isosbestic	23.57%	17.38%	16.88%	23.64%	13.92%	19.82%	14.21%	22.52%	25.59%	25.52%
Coefficient of Variation Artery Sensitive	32.98%	20.22%	21.68%	22.70%	18.63%	19.29%	15.31%	26.61%	18.31%	18.20%
Coefficient of Variation Vein Isosbestic	46.84%	29.46%	15.70%	25.17%	17.90%	7.22%	14.85%	16.32%	35.48%	32.90%
Coefficient of Variation Vein Sensitive	46.20%	25.78%	20.31%	22.78%	22.22%	14.03%	16.74%	26.04%	20.29%	24.14%
Coefficient of Variation Tissue Isosbestic	31.18%	23.54%	17.22%	16.74%	17.75%	13.56%	10.59%	18.96%	15.82%	22.22%
Coefficient of Variation Tissue Sensitive	39.06%	20.28%	20.01%	11.83%	19.19%	14.56%	11.26%	22.84%	23.47%	22.34%

the artery. The mean values of the averages of the light intensity within the respective bandwidths (isosbestic and oxygen sensitive) for each of the locations are presented in Tables 1 and 2 for each subject. Calculated OD values calculated for the perspective bandwidths for each location (tissue, artery, and vein) are presented in Tables 1 and 2. Arteriovenous ODR differences for each subject are listed in Tables 1 and 2, with positive values representing arterial blood oxygen saturation higher than venous oxygen saturation. The coefficient of variation for each of the intensity measurements for each subject was calculated; values are presented in Tables 1 and 2 for each subject. Arterial ODRs were significantly greater than venous ODRs (1.01 ± 2.61 and -1.43 ± 4.31 respectively; $p = 0.02$) (mean \pm standard deviation), suggesting higher oxygen saturation in arterial blood (Fig. 7). The average arteriovenous (AV) ODR differences were 2.44 ± 4.01 (mean \pm standard deviation), ranging from -2.19 to 13.73 .

5 Discussion

In the present study, we found that significant differences can be observed in spectral absorption between blood in arteries and veins in the back of the eye. Specifically, arterial ODRs were significantly greater than venous ODRs. One contributing factor to the observed difference may be a detectable higher concentration of oxygenated hemoglobin in retinal arteries than in retinal veins. However, since the entire a-scan was included in the analysis, it is possible that local variations in tissue pigmentation or any number of other factors existing outside of the blood column could have contributed to either the observed significant difference, or the high levels of variability observed. Indeed, until the contribution to noise and possible systematic error induced by the various steps involved in the processing and analysis of the data are quantified, it is impossible to confidently conclude that hemoglobin

Table 2 A continuation of Table 1, with mean and standard deviations presented for each of the variables across all subjects. The mean light intensity measurements as a percentage of CCD saturation are presented as an indication of signal intensity.

	Subject							All Subjects Mean	All Subjects Standard Deviation	% Total Potential Light
	11	12	13	14	15	16	17			
Mean Artery Isosbestic	41.59	22.54	61.26	37.98	53.80	49.74	45.34	45.30	14.30	0.012%
Mean Artery Sensitive	48.75	3.43	73.79	37.92	59.82	46.19	49.75	50.19	20.49	0.013%
Mean Vein Isosbestic	40.29	21.26	63.73	36.21	57.87	47.39	45.33	44.47	15.18	0.011%
Mean Vein Sensitive	47.47	3.64	72.68	39.59	58.67	50.18	50.07	50.08	20.42	0.013%
Mean Tissue Isosbestic	42.05	16.44	64.90	41.44	53.34	47.27	43.72	43.41	15.03	0.011%
Mean Tissue Sensitive	51.19	3.74	72.66	45.66	61.21	52.24	50.85	50.94	19.65	0.013%
OD Artery Isosbestic	0.01	-0.32	0.06	0.09	-0.01	-0.05	-0.04	-0.06	0.11	
OD Artery Sensitive	0.05	0.09	-0.02	0.19	0.02	0.12	0.02	0.02	0.09	
ODR Artery	4.44	-0.28	-0.27	2.13	-2.71	-2.41	-0.60	1.01	2.61	
OD Vein Isosbestic	0.04	-0.26	0.02	0.14	-0.08	0.00	-0.04	-0.03	0.09	
OD Vein Sensitive	0.08	0.03	0.00	0.14	0.04	0.04	0.02	0.03	0.08	
ODR Vein	1.77	-0.10	-0.02	1.06	-0.52	-16.15	-0.42	-1.43	4.31	
ODR Art—ODR Vein	2.68	-0.17	-0.25	1.07	-2.19	13.73	-0.18	2.44	4.01	
Coefficient of Variation Artery Isosbestic	19.46%	46.32%	19.37%	23.88%	28.19%	24.82%	28.14%			
Coefficient of Variation Artery Sensitive	17.94%	111.78%	27.29%	28.69%	16.23%	20.72%	17.29%			
Coefficient of Variation Vein Isosbestic	13.00%	30.11%	27.39%	34.11%	26.14%	29.65%	27.64%			
Coefficient of Variation Vein Sensitive	24.92%	182.92%	22.62%	46.06%	25.54%	25.38%	26.28%			
Coefficient of Variation Tissue Isosbestic	9.27%	62.73%	20.88%	28.05%	28.11%	19.58%	15.79%			
Coefficient of Variation Tissue Sensitive	16.98%	147.59%	19.27%	30.89%	26.43%	36.29%	12.98%			

oxygenation was the driving factor in the observed significant difference. Nevertheless, the present data do agree with the physical reality of higher oxygen saturation in arteries than in veins.

Another source of potential noise in the measurement is differing tissue content between a-scans primarily containing tissue and those containing blood large vessels. Figure 5 suggests that the retinal nerve fiber layer (RNFL) layer in tissue adjacent to large blood vessels may be thicker than the RNFL content in the volume of an a-scan that includes a large blood vessel. This difference in the content of backscattering materials in a-scans that the present study assumes to be similar may be contributing to the level of variability in the data.

A-scans were obtained near the vessel edges to avoid specular reflection that occurs near the center (Fig. 6). The intensity of specular reflection decreases as the OD measurements are obtained farther from the vessel center. However, the distance through the blood column also decreases as the

measurement distance from the vessel center increases. It is currently unknown if there is some critical level of specular reflection that must be avoided for meaningful OD measurements. For this reason, it is advised that OD measurements of blood columns be made near the edge of the vessel.³³

The utility of the measurements in the present study for oximetry depends on the linear relationship between ODR and oxygen saturation¹⁰; however, the applicability of ODR to oximetry measurements obtained from backscattered light has several limitations.³⁴ The Beer-Lambert law applies to transmission of light; and furthermore, the extinction coefficient values for light transmission through a solution of hemoglobin were obtained using hemolyzed blood.³⁴ The cells in whole blood as well as the surrounding tissue all create scatter, which is not accounted for in the Beer-Lambert model. Further work is necessary to provide more accurate estimates of the “extinction coefficient” as measured under conditions of light backscattered from whole blood in vessels embedded in

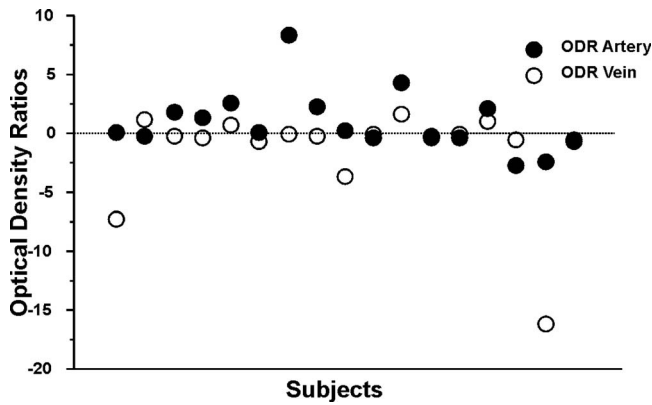


Fig. 7 Arterial ODRs were significantly greater than venous ODRs ($p=0.0217$), representing greater oxygen saturation in arteries than in veins. A large number of factors likely contributed to individual exceptions to the observed average difference between arterial and venous oxygen saturation, including a low signal-to-noise ratio, high variability, and a lack of compensation for scattering by blood cells and other retinal structures.

tissue and illuminated with a low-coherence superluminescent diode, as is the case in OCT imaging. Concerning the use of the OCT to estimate the intensity of backscattered light, previous techniques utilized film or digital cameras to integrate light backscattered from all reflective retinal sources regardless of tissue depth. The OCT limits the location of reflective signal sources to those contained within the a-scan. Measurement of backscattered light from nearly identical depths, as obtained when analyzing adjacent a-scans in an OCT frame, may be beneficial.

Coefficients of variation in intensity measurements were high, ranging from 7% to 183%, averaging 26%. For example, subject 12 presents with very large coefficients of variation. In this subject, the light levels in at least some of the measurements were very low (Table 2). While the average coefficient of variation was below 30%, the high variability in the level of variation may be due to the extremely low signal level. The average level of light intensity measurement was barely above 1/100th of 1% of the CCD saturation level.

The analysis of light backscattered by shadowed tissue contributes to the signal in at least three ways. First, light traveling to shadowed tissue must pass through the blood column. This light will have experienced scatter and absorption as a function of wavelength, altering the spectral intensity distribution before arriving at the tissue. Second, light backscattered from shadowed tissue must pass through the blood column a second time on the way to the spectrometer. This light will also experience wavelength-dependent scatter and absorption. Finally, unlike light backscattered directly from the blood column, it is possible that the optical qualities of the tissue may also alter the spectrum of backscattered light in a wavelength-dependent manner. This would be damaging to attempts to calculate an exact ODR based on the arterial or venous a-scan alone; however, the ODs calculated in the present study used light backscattered from adjacent a-scans containing nonshadowed tissue to represent the expected level of backscattered light in the absence of blood interactions. In this case, the local optical properties of shadowed and non-shadowed tissues are assumed to be equal, and their effect

removed in calculation of the OD ratio. In this context, the inclusion of shadowed tissue in the calculation of OD actually amplifies the effect of light/blood interaction by making measurements of backscattered light that has twice passed through the blood column.

The ultimate goal of Fourier domain OCT oximetry is to determine a precise numerical value for the percentage of oxygen saturation of blood within retinal arteries and veins. Unfortunately, these vessels are located adjacent to the photoreceptors and retinal pigment epithelium, each containing various pigments that may affect optical density measurements, and behind the vitreous. Light going to and from the vessels must interact with water within the vitreous (relevant in the near-IR range) and retinal pigments. In a previous study of retinal blood oxygenation measured in a two-wavelength spectral system (569 and 600 nm), arterial blood oxygen saturation was 97% and venous blood oxygen saturation was 55%.³⁰ In this study the authors corrected ODRs for individual influences of retinal pigments. The influence of spectral absorption in the near-IR wavelengths used in the present study has yet to be determined. It is possible that interindividual variations in pigments may have contributed to the variability observed in the absolute values in ODRs and differences in magnitude in AV ODR differences.

It is possible to calculate the expected loss of light in retinal arteries and veins based on known extinction coefficients. Substituting OD from Eq. (3) in Eq. (2) yields

$$OD = \varepsilon^* d^* C. \quad (5)$$

This makes the ODR used in the present study equal to

$$ODR = \frac{OD_{855}}{OD_{805}} = \frac{\varepsilon_{855}}{\varepsilon_{805}}. \quad (6)$$

Since the scattering effect of hemoglobin is dominant above wavelengths of approximately 600 nm, it bears repeating that the extinction coefficient combines both absorption and scattering effects. With $\varepsilon_{855} \text{ oxyhemoglobin} = 1073$, $\varepsilon_{855} \text{ deoxyhemoglobin} = 691$, $\varepsilon_{805} \text{ isosbestic} = 797$, and assuming a 55% saturation in venous blood³⁰ and 100% saturation in the arteries, arterial ODRs should be approximately 1.2 times greater than in veins. Our data demonstrated a wide variation in the difference between arterial and venous ODRs. It is possible that this is due to the effects of pigments and water absorption, which were not corrected for, or it may also be due to a variation in venous blood saturation within this experimental cohort.

Differential absorption by water also contributed to differences in ODs between 805 and 855 nm. The extinction coefficient of water increases by approximately 300% in the 800- to 900-nm range, the bandwidth of our light source. The effect of water was constant between arteries and veins, since the approximate distance through the vitreous and anterior structures to adjacent vessels and tissue is the same; nevertheless, the contribution of water absorption will need to be taken into account before actual saturation values can be calculated.

In conclusion, this pilot study utilized a two-wavelength ODR approach similar to a previous publication with a fundus camera-based system. Calculating an ODR between 855 and 805 nm, we detected a statistically significant difference in

arterial and venous ODRs, which is consistent with the known difference between arterial and venous blood oxygen saturation, a difference known to exist *a priori*. Future refinements include spatial localization of measurements to relevant tissues (e.g., intravascular), correcting for the absorption of retinal pigments and water, and utilizing the entire available bandwidth to increase accuracy and precision of hsUHR-OCT oximetry.

References

1. R. Y. Foos, "Regional ischemic infarcts of the retina," *Albrecht von Graefes Arch. Klin. Exp. Ophthalmol.* **200**, 183–194 (1976).
2. M. Shimo-Oku and S. Miyazaki, "Acute anterior and posterior ischemic optic neuropathy," *Jpn. J. Ophthalmol.* **28**, 159–170 (1984).
3. S. S. Hayreh and P. Podhajsky, "Ocular neovascularization with retinal vascular occlusion. II. Occurrence in central and branch retinal artery occlusion," *Arch. Ophthalmol. (Chicago)* **100**, 1585–1596 (1982).
4. R. A. Ashman, F. Reinholz, and R. H. Eikelboom, "Oximetry with a multiple wavelength SLO," *Int. Ophthalmol.* **23**, 343–346 (2001).
5. J. P. de Kock, L. Tarassenko, C. J. Glynn, and A. R. Hill, "Reflectance pulse oximetry measurements from the retinal fundus," *IEEE Trans. Biomed. Eng.* **40**, 817–823 (1993).
6. S. H. Hardarson, A. Harris, R. A. Karlsson, et al., "Automatic retinal oximetry," *Invest. Ophthalmol. Visual Sci.* **47**, 5011–5016 (2006).
7. J. B. Hickam and J. C. Ross, "An improved method for photographic measurement of retinal venous blood oxygen," *Tech. Doc. Rep. SAMTDR USAF Sch. Aerosp. Med.* **62–64**, 5p.:5p (1962).
8. J. B. Hickam, R. Frayser, and J. C. Ross, "A study of retinal venous blood oxygen saturation in human subjects by photographic means," *Circulation* **27**, 375–385 (1963).
9. J. Sebag, F. C. Delori, G. T. Feke, and J. J. Weiter, "Effects of optic atrophy on retinal blood flow and oxygen saturation in humans," *Arch. Ophthalmol. (Chicago)* **107**, 222–226 (1989).
10. J. S. Tiedeman, S. E. Kirk, S. Srinivasan, and J. M. Beach, "Retinal oxygen consumption during hyperglycemia in patients with diabetes without retinopathy," *Ophthalmology* **105**, 31–36 (1998).
11. D. J. Faber, E. G. Mik, M. C. Aalders, and T. G. van Leeuwen, "Light absorption of (oxy-)hemoglobin assessed by spectroscopic optical coherence tomography," *Opt. Lett.* **28**, 1436–1438 (2003).
12. D. J. Faber, M. C. Aalders, E. G. Mik, B. A. Hooper, M. J. van Gemert, and T. G. van Leeuwen, "Oxygen saturation-dependent absorption and scattering of blood," *Phys. Rev. Lett.* **93**, 028102 (2004).
13. D. J. Faber, E. G. Mik, M. C. Aalders, and T. G. van Leeuwen, "Toward assessment of blood oxygen saturation by spectroscopic optical coherence tomography," *Opt. Lett.* **30**, 1015–1017 (2005).
14. M. M. Frojmovic and R. Panjwani, "Blood cell structure-function studies: light transmission and attenuation coefficients of suspensions of blood cells and model particles at rest and with stirring," *J. Lab. Clin. Med.* **86**, 326–343 (1975).
15. C. Pitris, M. E. Brezinski, B. E. Bouma, G. J. Tearney, J. F. Southern, and J. G. Fujimoto, "High resolution imaging of the upper respiratory tract with optical coherence tomography: a feasibility study," *Am. J. Respir. Crit. Care Med.* **157**, 1640–1644 (1998).
16. X. D. Li, S. A. Boppart, D. J. Van, et al., "Optical coherence tomography: advanced technology for the endoscopic imaging of Barrett's esophagus," *Endoscopy* **32**, 921–930 (2000).
17. W. Drexler, H. Sattmann, B. Hermann, et al., "Enhanced visualization of macular pathology with the use of ultrahigh-resolution optical coherence tomography," *Arch. Ophthalmol. (Chicago)* **121**, 695–706 (2003).
18. M. Gloesmann, B. Hermann, C. Schubert, H. Sattmann, P. K. Ahnelt, and W. Drexler, "Histologic correlation of pig retina radial stratification with ultrahigh-resolution optical coherence tomography," *Invest. Ophthalmol. Visual Sci.* **44**, 1696–1703 (2003).
19. A. Unterhuber, B. Povazay, B. Hermann, et al., "Compact, low-cost Ti:Al₂O₃ laser for in vivo ultrahigh-resolution optical coherence tomography," *Opt. Lett.* **28**, 905–907 (2003).
20. E. M. Anger, A. Unterhuber, B. Hermann, et al., "Ultrahigh resolution optical coherence tomography of the monkey fovea. Identification of retinal sublayers by correlation with semithin histology sections," *Exp. Eye Res.* **78**, 1117–1125 (2004).
21. W. Drexler, "Ultrahigh-resolution optical coherence tomography," *J. Biomed. Opt.* **9**, 47–74 (2004).
22. W. Drexler, "Methodological advancements. Ultrahigh-resolution OCT," *Ophthalmologe* **101**, 804–812 (2004).
23. M. Wojtkowski, R. Leitgeb, A. Kowalczyk, T. Bajraszewski, and A. F. Fercher, "In vivo human retinal imaging by Fourier domain optical coherence tomography," *J. Biomed. Opt.* **7**, 457–463 (2002).
24. M. Wojtkowski, V. Srinivasan, J. G. Fujimoto, et al., "Three-dimensional retinal imaging with high-speed ultrahigh-resolution optical coherence tomography," *Ophthalmology* **112**, 1734–1746 (2005).
25. D. C. Adler, T. H. Ko, and J. G. Fujimoto, "Speckle reduction in optical coherence tomography images by use of a spatially adaptive wavelet filter," *Opt. Lett.* **29**, 2878–2880 (2004).
26. R. Huber, D. C. Adler, and J. G. Fujimoto, "Buffered Fourier domain mode locking: unidirectional swept laser sources for optical coherence tomography imaging at 370,000 lines/s," *Opt. Lett.* **31**, 2975–2977 (2006).
27. V. J. Srinivasan, M. Wojtkowski, A. J. Witkin, et al., "High-definition and 3-dimensional imaging of macular pathologies with high-speed ultrahigh-resolution optical coherence tomography," *Ophthalmology* **113**, 2054.e1–14 (2006).
28. M. Wojtkowski, T. Bajraszewski, P. Targowski, and A. Kowalczyk, "Real-time in vivo imaging by high-speed spectral optical coherence tomography," *Opt. Lett.* **28**, 1745–1747 (2003).
29. M. Wojtkowski, T. Bajraszewski, I. Gorczynska, et al., "Ophthalmic imaging by spectral optical coherence tomography," *Am. J. Ophthalmol.* **138**, 412–419 (2004).
30. J. M. Beach, K. J. Schwenzer, S. Srinivasan, D. Kim, and J. S. Tiedeman, "Oximetry of retinal vessels by dual-wavelength imaging: calibration and influence of pigmentation," *J. Appl. Physiol.* **86**, 748–758 (1999).
31. M. Crittin, H. Schmidt, and C. E. Riva, "Hemoglobin oxygen saturation (So₂) in the human ocular fundus measured by reflectance oximetry: preliminary data in retinal veins," *Klin. Monatsbl. Augenheilkd.* **219**, 289–291 (2002).
32. S. Wray, M. Cope, D. T. Delpy, J. S. Wyatt, and E. O. Reynolds, "Characterization of the near infrared absorption spectra of cytochrome aa₃ and haemoglobin for the non-invasive monitoring of cerebral oxygenation," *Biochim. Biophys. Acta* **933**, 184–192 (1988).
33. H. Narasimha-Iyer, J. M. Beach, B. Khoobehi, J. Ning, H. Kawano, and B. Roysam, "Algorithms for automated oximetry along the retinal vascular tree from dual-wavelength fundus images," *J. Biomed. Opt.* **10**, 54013 (2005).
34. F. C. Delori, "Noninvasive technique for oximetry of blood in retinal vessels," *Appl. Opt.* **27**, 1113–1125 (1988).